Supplementary Materials for

Seafloor microplastic hotspots controlled by deep-sea circulation

Ian A. Kane*, Michael A. Clare, Elda Miramontes, Roy Wogelius,
James J. Rothwell, Pierre Garreau, Florian Pohl

*Corresponding author. Email: ian.kane@manchester.ac.uk

Published 30 April 2020 on *Science* First Release
DOI: 10.1126/science.aba5899

This PDF file includes:

Other Supplementary Material for this manuscript includes the following:
(available at science.sciencemag.org/cgi/content/full/science.aba5899/DC1)

Data S1 (.xlsx)

Materials and Methods

Geophysical data

The regional bathymetry for the Tyrrhenian Sea is based on the 2018 EMODnet digital terrain model (DTM), which has a resolution of 0.125 arc-minutes (c. 180 x 230 m bins). Data were downloaded from the EMODnet portal at: http://doi.org/10.12770/18ff0d48-b203-4a65-94a9-5fd8b0ec35f6. Local bathymetry was acquired in 2008 using a shipboard EM300 multibeam echo sounder (25 m x 25 m bin size) from the M/V Geoprospector and from the S/V Echo Surveyor Hugin 3000 Autonomous Under Water Vehicle (AUV) equipped with a Simrad EM2000 multibeam echosounder (1 m x 1 m bin size). Raster surfaces were created from the gridded bathymetry data in ArcGIS v10.0 in order to visualise the seafloor, identify the different physiographic domains and select the location of sediment cores. Multichannel Ultra High Resolution (UHR) 2D seismic data were also acquired from the M/V Geoprospector in 2008 to image the subsurface geology. The seismic survey used a Sleeve Gun Array with 20 Cubic inch array volume and an energy of 2000 PSI, towed at a water depth of 1.0 +/- 0.5 m with a shot interval of 12.5 m. The Teledyne streamer is 300 m in length with 24 hydrophone groups at an interval of 12.5 m at the same tow depth, typical fold of 12 (12 reflections per trace). These UHR data were obtained to a depth of approximately 2000 m below seafloor and clearly show diagnostic features of contourite deposition, which has occurred since the Pliocene (*31*) (Fig. 1D). We use these seafloor and subsurface data to identify the main physiographic domains: i) continental shelf; ii) continental slope; iii) areas of preferential (mounded and plastered drifts) and inhibited sediment accumulation (moats) due to the influence of bottom currents; and iii) structurally-controlled mid-slope basins (Figs. 1D, 2E & 3C).

Sediment sampling

A total of 16 sediment cores were collected from the M/V Commander in 2008 to characterize the different physiographic domains in the study area. Cores of up to 0.5 m length were extracted from a 27-litre self-triggering box corer, which allowed an undisturbed sediment-water interface to be preserved. Samples were immediately sealed to minimize airborne contamination. Positioning was determined using an Ultra Short Baseline (USBL) attached to the box-corer frame, which has a horizontal accuracy of approximately 0.2 m.

Microplastic extraction

Here we follow established approaches (*55, 56*), and other subsequent prominent investigations of microplastics (e.g. *10, 11*, *57-61*) who suggested that microplastic should refer to microplastic fragments with a longest dimension of <1 mm. This is logical as 'micro' generally refers to the micrometer size range,

and this size class predominates in marine environments. Microplastic fibers typically have lengths of 50 μm up to a few mm, and a diameter of <10-30 μm. For the purpose of this study (where optical identification of microplastics was the aim), only particles >63 μm were analyzed, since smaller microplastic particles could not be reliably identified (*59*). Microplastics were isolated from clay-silt grade sediment using a disaggregation and dense-fluid settling approach. In order to ensure comparison with other studies, published protocols were followed. Sediment cores were handled by individuals wearing only natural fiber clothing, wearing cotton laboratory coats and headwear, and latex gloves (following (*20*)). Prior to sediment sampling, cores had been stored in refrigerated conditions. A sub-sample of each sediment core was extracted with a wet-weight of 54.2 - 69.92 g. Samples had a surface area of approximately 1–3 cm^2 x 5–8 cm deep. Seafloor samples have variable water content so they were dried to create samples weighing 50 g; for comparative purposes samples and their microplastic content are normalized to 50 g. Sediment samples were stored in aluminum foil and kept refrigerated. Samples were disaggregated in a clean lab using a magnetic stirrer in $ZnCl_2$ solution (1.7 g m^{-3}). Microplastics were extracted using a Sediment-Microplastic-Isolation (SMI) unit (settling tube with ball valve to isolate the supernaut) following a modified protocol specifically developed for microplastic extraction (*60*) to ensure comparability between studies. The SMI unit was thoroughly rinsed using deionized water prior to use. Following settling, the supernaut fluid was poured from the closed SMI unit, rinsed with deionized water to flush any remaining microplastics, and vacuum filtered over a 20 μm filter. The filters were then placed into glass petri dishes and immediately covered. They were then dried and analyzed using optical microscopy. Procedural blanks were made at each stage but only yielded 2 plastic microfibers, of unknown source, in the entire experiment (where a total of 957 particles were extracted); several cotton fibers were confirmed during the experiment (confirmed by hot needle test). Microplastics are readily identified by eye, as having an unnatural appearance and bright colors; these were confirmed using the 'hot needle test' (following (*46*)). A subset of the confirmed microplastics were further analyzed using Fourier-transform infrared spectroscopy (FTIR) to establish polymer types and potential origin (following (*46*)).

The dried filter papers were analyzed in a clean microscopy lab using a Zeiss Axio Zoom.V1 stereomicroscope at 20–50× magnification. Filters were traversed systematically to identify microplastics which were visually identified by following the criteria (*46*): (1) no visible organic structures (*59*); (2) a positive reaction to the hot needle test (*58*); and (3) maintenance of structural integrity when touched or moved. We up-scaled the measured microplastic concentrations from the core sub-samples (representing a 5 cm thick layer with a surface area of 1 x 1 cm), to give a value per meter squared to enable comparison with other studies (Table S1).

Polymer identification

A wide variety of plastic polymers are produced by industry, and these materials undergo breakdown reactions when exposed to weathering processes. Oxidation of reduced carbon is a key reaction in the breakdown pathway, such that the quantity of oxygen-bearing functional groups in deposited plastics has been suggested as a possible breakdown index (*62*); the higher the oxygen inventory the more degraded the plastic. This degradation mirrors the breakdown pathways of natural organic carbon material deposited in sedimentary rocks, where oxidative processes convert pristine reduced carbon compounds such as collagen or keratin to more oxidized and less polymerized molecular fragments (*21*). As with natural material however, the range in composition and structure of plastics is wide and covers many different polymers. Therefore, analytical methods are required in order to characterize such material and reliably determine the degree of degradation. Infra-red methods are ideal for identifying diagnostic functional groups, determining the most probable original plastic, and then providing information about degree of degradation based on compositional differences between probable starting materials and the material recovered from the field (*63*). A subset (n=30) of the extracted microplastics was analyzed using Fourier transform infrared (FT-IR) spectroscopy, to confirm a polymer origin and to assess the degree of degradation. The FTIR spectrum range was set at 4,000–650 cm^{-1}, with a resolution of 4 cm^{-1}. Data were processed and diagnostic functional groups were identified using a standard reference library (Bio-Rad KnowItAll FTIR database, Academic Edition 2019). The resultant spectra produced from these samples were then compared with reference data from a comprehensive Attenuated Total Reflectance Polymer study of plastic marine debris (*63*) to assign polymer type and assess degree of degradation (Fig. S2).

Sediment grain size

Sediment sub-samples were analyzed using a Malvern Mastersizer 3000 and Hydro LV liquid handling unit, using water as the dispersant. The samples were subjected to a small amount of ultrasonic and pre-measurement dispersion. Three aliquots of each sample were analyzed, each measurement being analyzed five times sequentially, to confirm there was complete dispersion of the sample. The average of these five measurements is reported. The particle size distribution was modeled using a Fraunhofer estimation model. This is usually less accurate when compared to Mie Theory models (particularly at particle sizes <10 μm) but is appropriate in situations where a sample is made up of heterogeneous material, so the optical properties cannot be calculated. All samples were muds, dominated by clay and silt, with a minor component of shell fragments, particularly in the shelf and plastered contourite drift samples, and predominantly in the lower-fine-grained silt range (Fig. S3). Grain size of the mean sortable silt has been calculated (i.e. grain sizes >10 μm) to allow comparison to other studies (following *64*) (Fig. S3).

Global comparison of seafloor microplastic concentration

In order to compare measured microplastic concentrations from the samples in the Tyrrhenian Sea with other sites, we compiled data from publications that provided details on the depositional environment (Fig. 2). These include continental shelves, open continental slopes, submarine canyons, abyssal plains, ocean trenches and seamounts (*11*, *20, 27, 37, 38, 65-69*).

Oceanographic and particle transport modeling

Hydrodynamic modeling of the bottom current circulation patterns was used to explore the near-bed flow velocities and shear stresses exerted on the seafloor (Fig. S4). The MARS3D (3D hydrodynamical Model for Applications at Regional Scale) model was used to simulate coastal and regional circulation (developed by (*69, 70, 31*)). We used the "MENOR" configuration of the MARS3D model, which has a horizontal resolution of 1200 m in the north Tyrrhenian Sea. The model simulates currents, temperature and salinity on 60 vertical levels using a generalized sigma coordinate system (*31*). Initial and boundary conditions were calibrated using the HYMEX observation experiment conducted in the NW Mediterranean from summer 2012 to spring 2013 (*71*). The bottom current velocity was characterized by the friction velocity:

$$u^* = \frac{\kappa u(z)}{ln(\frac{z}{z_0})}$$

where κ is the von Kármán constant (equal to 0.4 (*72*), z^0 the bottom roughness length taken here to a constant equal to 0.0035 m and *z* the distance from the bottom where the current velocity *u(z)* is computed (*31*). The shear stress (τ) generated by currents at the seafloor is related to the sea water density (ρ) and the friction velocity (u^*) and was computed over the thickness of the bottom layer thickness using:

$$\tau = \rho u^{*2}$$

We present the 90th percentile of the near-bed shear stress in order to remove extreme and transitory events.

Bed shear stresses are then used to calculate Shields numbers and boundary Reynolds numbers for different particle sizes.

Dimensionless shear stress (τ^*) is calculated as:

$$\tau^* = \frac{\tau}{(\rho_s - \rho_w)gD}$$

Where τ is shear stress, g is acceleration due to gravity, ρ_s is the particle density, ρ_w is the fluid density (1029 kg m^{-3}) and D is the particle diameter.

Boundary Reynolds (R_*) number is determined from:

$$R_* = \frac{u_* D}{\nu}$$

Wherein ν is kinematic viscosity and shear velocity (u_*) is calculated as:

$$u_* = \sqrt{\frac{\tau}{\rho_w}}$$

We show calculations to represent i) the range of microplastics identified in the sediment cores, including three sizes (1.0, 0.5, and 0.1 mm) and two polymers (based on results of the FTIR analysis) with different densities (polyethylene, ρ=1380 kg m^{-3}; nylon, ρ=1150 kg m^{-3}) and ii) the range of sediment grain sizes sampled in the cores (D^{90}=0.014-0.121 mm). By plotting the results on a Shields diagram (Fig. 4), it can be seen that under the range of bed shear stresses observed in the model outputs (Fig. S4) that the host sediments are likely to be stable and not moved. Nylon is more prone to mobilization, typically moving at bed shear stresses of c. 0.03-0.04 N m^{-2} and may become suspended at shear stresses >0.1 N m^{-2}.These values correspond well with the observed abundance of microplastics (both fibers and fragments) in relation to the bed shear stresses determined from numerical modeling (Fig. S5).

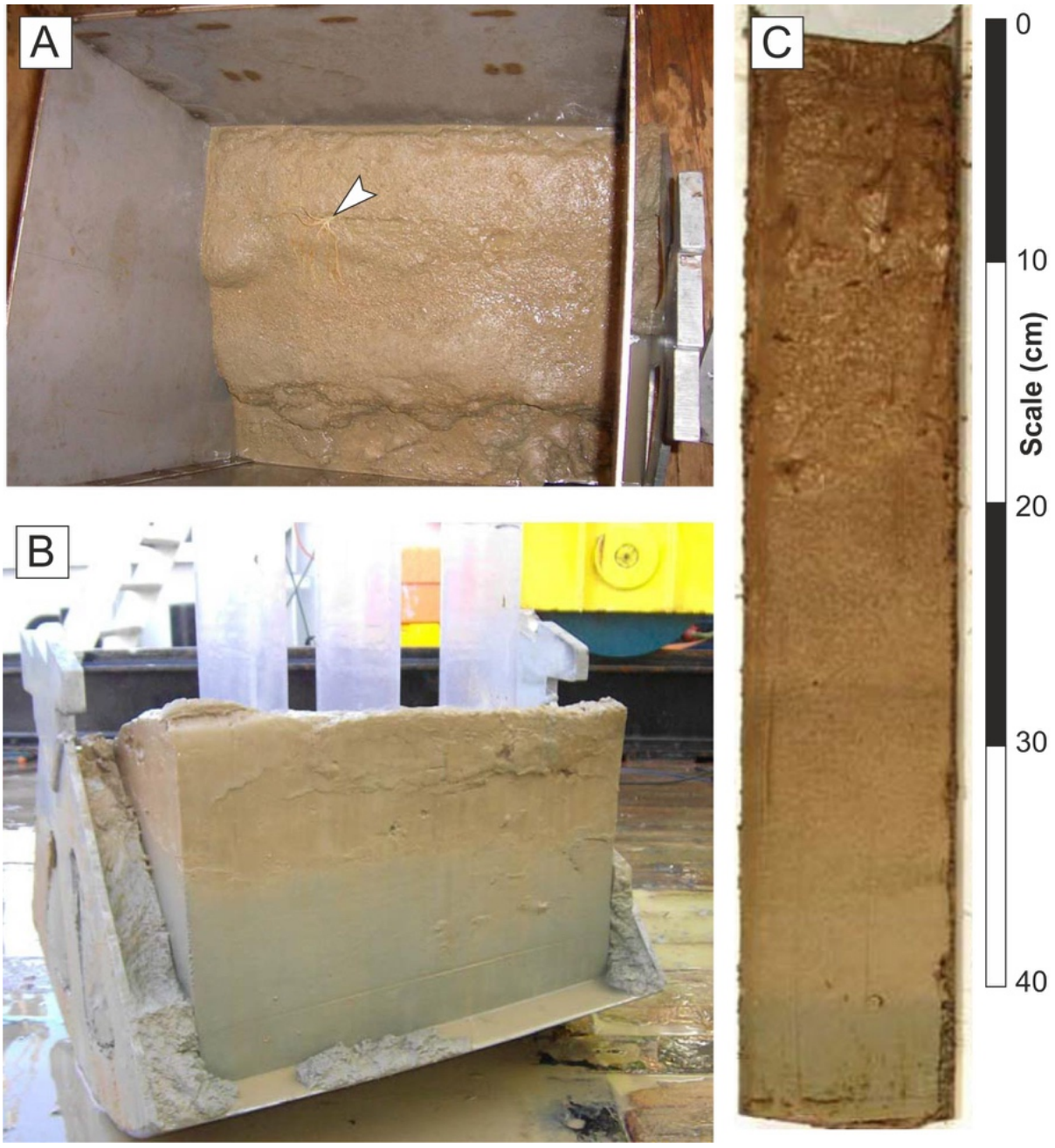

Fig. S1. A) Example of undisturbed sediment-water interface preserved in a box core (Sample 9). The arrow indicates a brittle star (echinoderm). B) Example of box core immediately after extraction, with sediment core tubes inserted (Sample 11). C) Example of split sediment core extracted from box core (Sample 7). Scale = centimeters. Note sediment cores used in this study were not split, in order to minimize airborne contamination; hence this is one of multiple cores taken from the box corer.

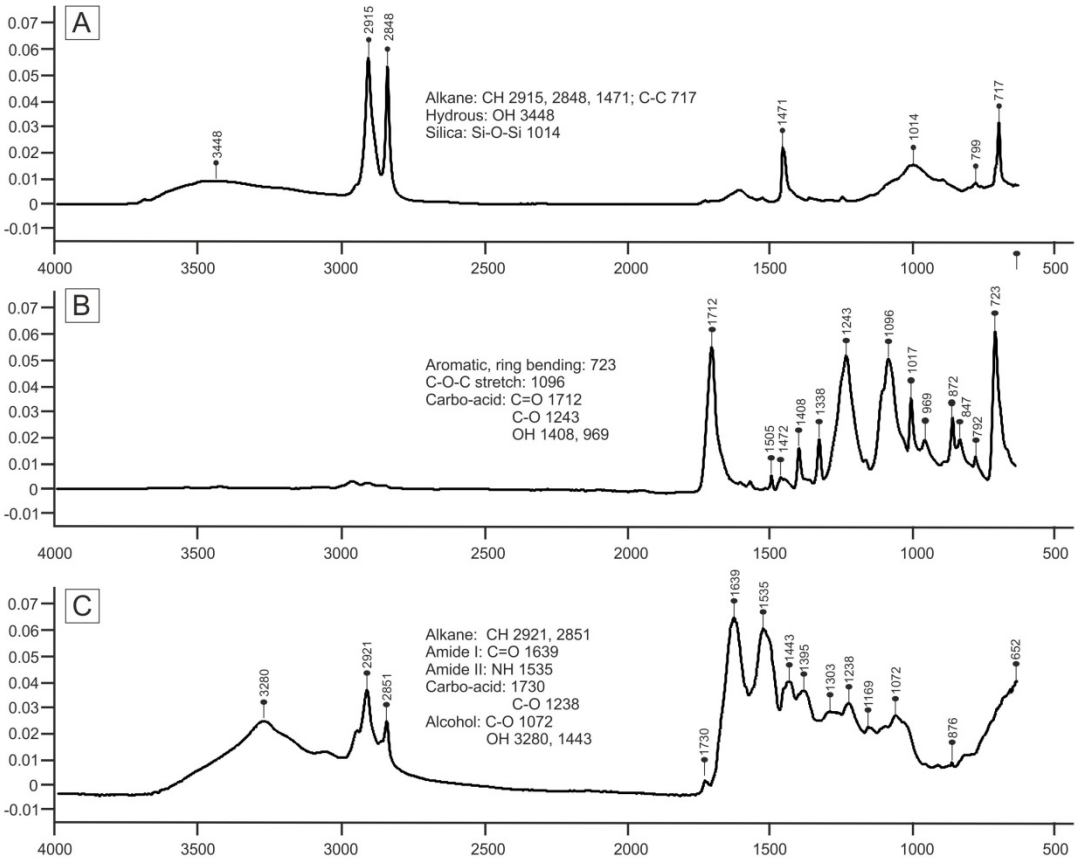

Fig. S2. FTIR spectra from three different types of plastic resolved in the subset of samples A) polyethylene, B) polyethylene terephthalate, and C) nylon. The nylon is judged to be the most degraded because it displays the most hydration and largest relative peak intensity shifts when compared to published spectra of pristine material. The two other samples are less degraded.

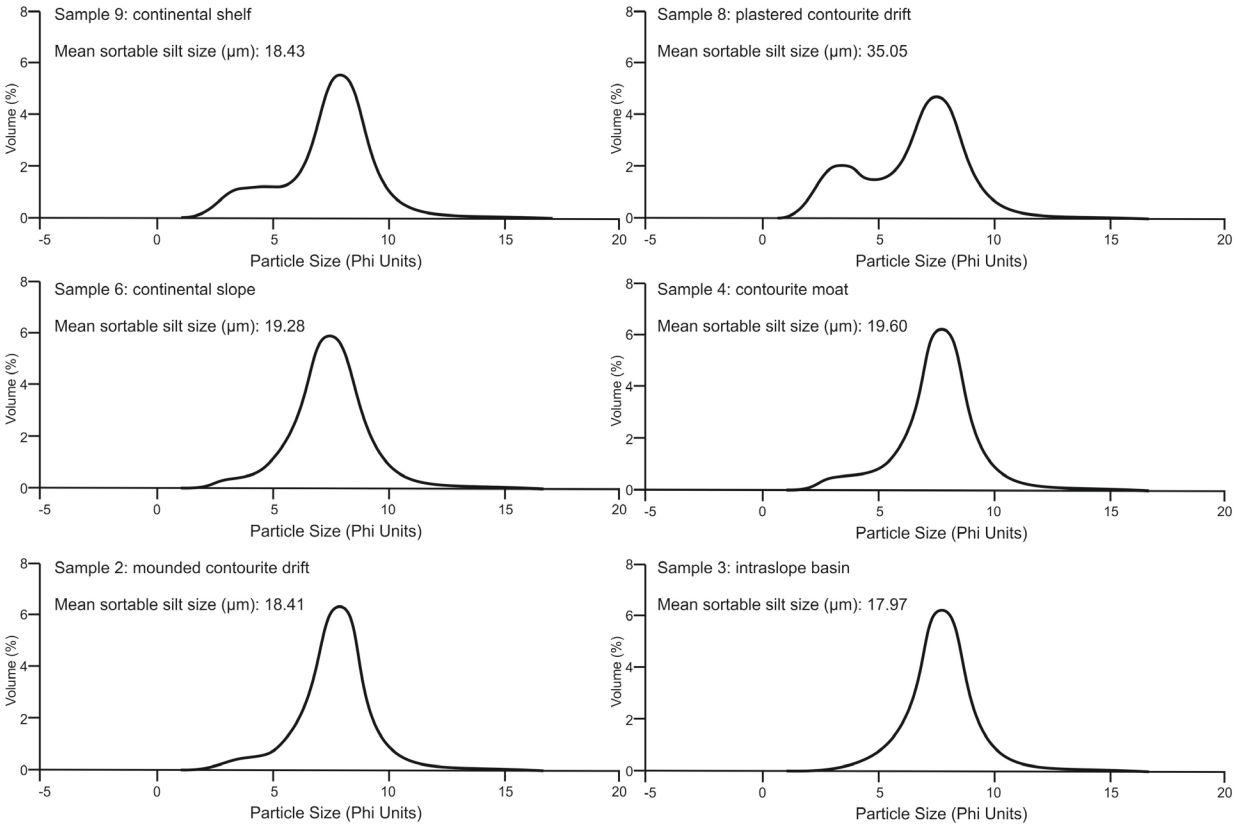

Fig. S3. Grain size distribution of sediment samples in each physiographic domain.

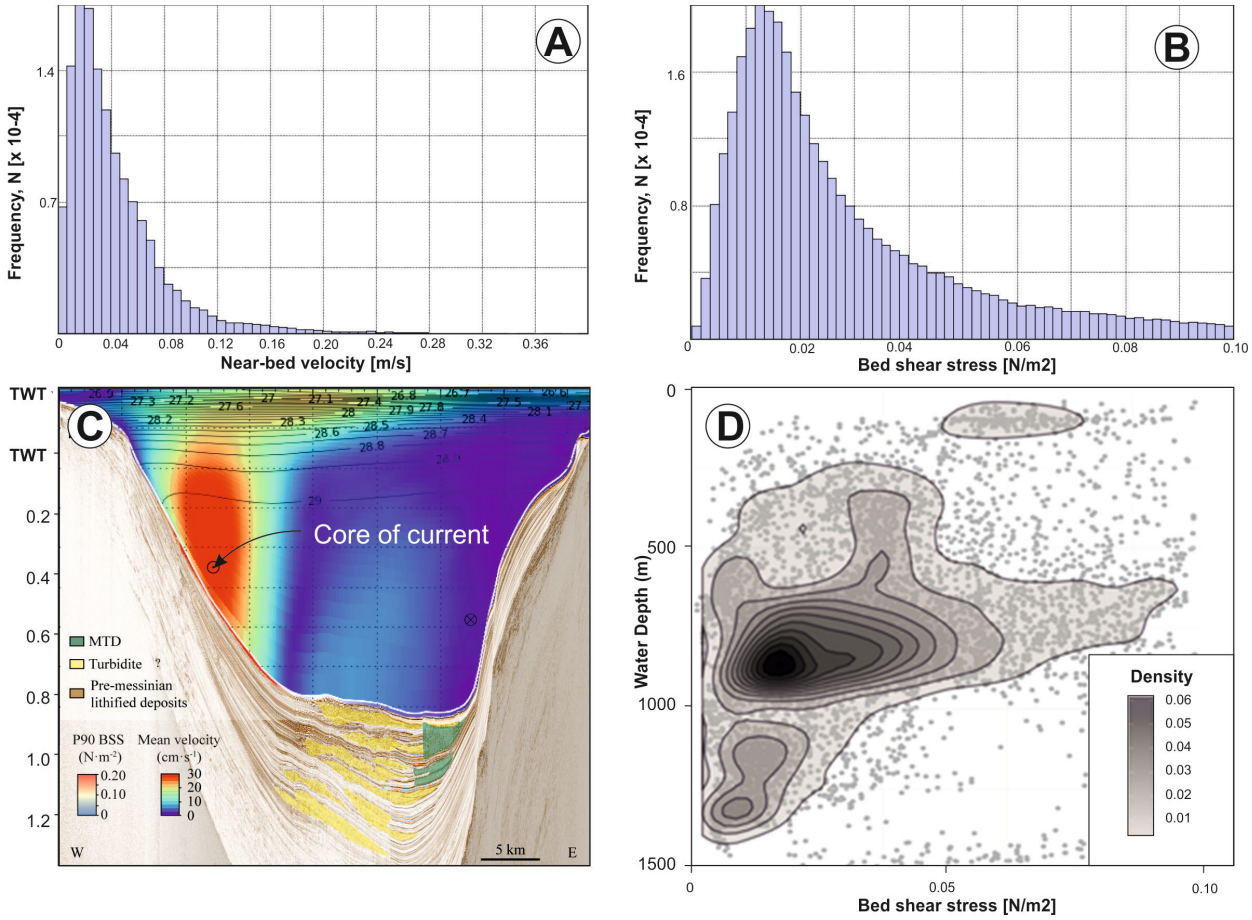

Fig. S4. Frequency histograms illustrating the range of simulated (A) near-bed velocity and (B) bed shear stress from the modeling across the study area. Example output from model showing modelled water velocities and bed shear stresses (C) in summer situation when the core of the current is intensified along the western flank of the basin between distinct water depth ranges (modified after (31)). MTD refers to Mass Transport Deposit. BSS=bed shear stress. (D) 2D kernel density plot showing how bed shear stresses within the study are most focused within the water depth range of c.600-900 m.

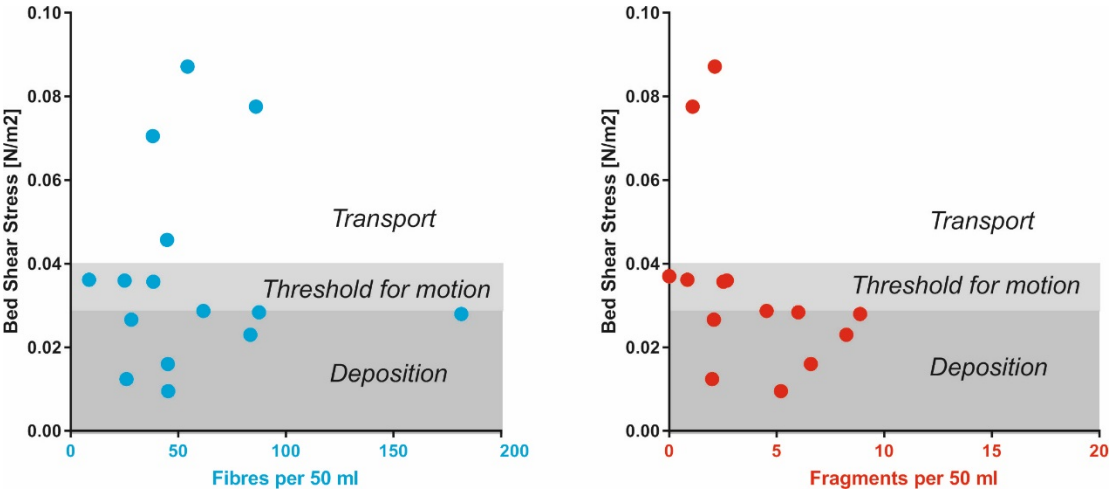

Fig. S5. Bed shear stresses at each of the sampled locations plotted against concentration of fibers (left) and fragments (right). Grey background fills annotate whether deposition or transport is expected based on the outputs from Fig. 4. It can be seen that microplastic fragment abundance generally increases with shear stress to a threshold level (c. 0.03 N m^{-2}), above which there is a decrease in abundance. Microfibers are less strongly affected.

Sample Name	Microplastic Type	Physiographic Domain	Total	per 50 g	%fibers	%particles	Pieces per m^2
1	Fibers	Intra slope basin	45	45	90	10	452792
1	Fragments	Intra slope basin	5	5			50310
2	Fibers	Mounded drift	102	88	94	6	875286
2	Fragments	Mounded drift	7	6			60069
3	Fibers	Intra slope basin	26	26	93	7	259265
3	Fragments	Intra slope basin	2	2			19943
4	Fibers	Moat	43	45	93	7	447683
4	Fragments	Moat	3	3			31234
5	Fibers	Mounded drift	48	45	87	13	451552
5	Fragments	Mounded drift	7	7			65851
6	Fibers	Mounded drift	184	182	95	5	1815491
6	Fragments	Mounded drift	9	9			88801
7	Fibers	Mounded drift	81	83	91	9	834335
7	Fragments	Mounded drift	8	8			82403
8	Fibers	Plastered drift	79	86	99	1	860723
8	Fragments	Plastered drift	1	1			10895
9	Fibers	Shelf	43	38	93	7	383929
9	Fragments	Shelf	3	3			26786
10	Fibers	Mid slope	30	25	91	9	250000
10	Fragments	Mid slope	3	3			25000
11	Fibers	Upper slope	10	8	91	9	84746
11	Fragments	Upper slope	1	1			8475
12	Fibers	Plastered drift	32	38	70	30	380952
12	Fragments	Plastered drift	14	17			166667
13	Fibers	Plastered drift	51	54	96	4	542553
13	Fragments	Plastered drift	2	2			21277
14	Fibers	Mounded drift	68	62	93	7	616780
14	Fragments	Mounded drift	5	5			45351
15	Fibers	Moat	16	15	100	0	149827
15	Fragments	Moat	0	0			0
16	Fibers	Moat	27	28	90	10	281250
16	Fragments	Moat	3	3			31250

Table S1. Summary of microplastics identified (full results provided in supplementary spreadsheet (*54*)).

Data S1. (*54*)
Excel file with numbers and colors of fibres.

References and Notes

1. M. L. Taylor, C. Gwinnett, L. F. Robinson, L. C. Woodall, Plastic microfibre ingestion by deep-sea organisms. *Sci. Rep.* **6**, 33997 (2016). doi:10.1038/srep33997 Medline

2. M. Eriksen, L. C. M. Lebreton, H. S. Carson, M. Thiel, C. J. Moore, J. C. Borerro, F. Galgani, P. G. Ryan, J. Reisser, Plastic pollution in the world's oceans: More than 5 trillion plastic pieces weighing over 250,000 tons afloat at sea. *PLOS ONE* **9**, e111913 (2014). doi:10.1371/journal.pone.0111913 Medline

3. E. van Sebille, C. Wilcox, L. Lebreton, N. Maximenko, B. D. Hardesty, J. A. van Franeker, M. Eriksen, D. Siegel, F. Galgani, K. L. Law, A global inventory of small floating plastic debris. *Environ. Res. Lett.* **10**, 124006 (2015). doi:10.1088/1748-9326/10/12/124006

4. J. R. Jambeck, R. Geyer, C. Wilcox, T. R. Siegler, M. Perryman, A. Andrady, R. Narayan, K. L. Law, Plastic waste inputs from land into the ocean. *Science* **347**, 768–771 (2015). doi:10.1126/science.1260352 Medline

5. R. Geyer, J. R. Jambeck, K. L. Law, Production, use, and fate of all plastics ever made. *Sci. Adv.* **3**, e1700782 (2017). doi:10.1126/sciadv.1700782 Medline

6. L. C. M. Lebreton, J. van der Zwet, J.-W. Damsteeg, B. Slat, A. Andrady, J. Reisser, River plastic emissions to the world's oceans. *Nat. Commun.* **8**, 15611 (2017). doi:10.1038/ncomms15611 Medline

7. R. C. Thompson, Y. Olsen, R. P. Mitchell, A. Davis, S. J. Rowland, A. W. G. John, D. McGonigle, A. E. Russell, Lost at sea: Where is all the plastic? *Science* **304**, 838–838 (2004). doi:10.1126/science.1094559 Medline

8. A. A. Koelmans, M. Kooi, K. L. Law, E. van Sebille, All is not lost: Deriving a top-down mass budget of plastic at sea. *Environ. Res. Lett.* **12**, 114028 (2017). doi:10.1088/1748-9326/aa9500

9. C. A. Choy, B. H. Robison, T. O. Gagne, B. Erwin, E. Firl, R. U. Halden, J. A. Hamilton, K. Katija, S. E. Lisin, C. Rolsky, K. S. Van Houtan, The vertical distribution and biological transport of marine microplastics across the epipelagic and mesopelagic water column. *Sci. Rep.* **9**, 7843 (2019). doi:10.1038/s41598-019-44117-2 Medline

10. L. Van Cauwenberghe, L. Devriese, F. Galgani, J. Robbens, C. R. Janssen, Microplastics in sediments: A review of techniques, occurrence and effects. *Mar. Environ. Res.* **111**, 5–17 (2015). doi:10.1016/j.marenvres.2015.06.007 Medline

11. A. Vianello, A. Boldrin, P. Guerriero, V. Moschino, R. Rella, A. Sturaro, L. Da Ros, Microplastic particles in sediments of Lagoon of Venice, Italy: First observations on occurrence, spatial patterns and identification. *Estuar. Coast. Shelf Sci.* **130**, 54–61 (2013). doi:10.1016/j.ecss.2013.03.022

12. V. Zitko, M. Hanlon, Another source of pollution by plastics: Skin cleaners with plastic scrubbers. *Mar. Pollut. Bull.* **22**, 41–42 (1991). doi:10.1016/0025-326X(91)90444-W

13. S. A. Mason, D. Garneau, R. Sutton, Y. Chu, K. Ehmann, J. Barnes, P. Fink, D. Papazissimos, D. L. Rogers, Microplastic pollution is widely detected in US municipal

wastewater treatment plant effluent. *Environ. Pollut.* **218**, 1045–1054 (2016). doi:10.1016/j.envpol.2016.08.056 Medline

14. M. A. Browne, P. Crump, S. J. Niven, E. Teuten, A. Tonkin, T. Galloway, R. Thompson, Accumulation of microplastic on shorelines worldwide: Sources and sinks. *Environ. Sci. Technol.* **45**, 9175–9179 (2011). doi:10.1021/es201811s Medline

15. A. L. Andrady, Microplastics in the marine environment. *Mar. Pollut. Bull.* **62**, 1596–1605 (2011). doi:10.1016/j.marpolbul.2011.05.030 Medline

16. X. Tubau, M. Canals, G. Lastras, X. Rayo, J. Rivera, D. Amblas, Marine litter on the floor of deep submarine canyons of the Northwestern Mediterranean Sea: The role of hydrodynamic processes. *Prog. Oceanogr.* **134**, 379–403 (2015). doi:10.1016/j.pocean.2015.03.013

17. E. D. Goldberg, Plasticizing the seafloor: An overview. *Environ. Technol.* **18**, 195–201 (1997). doi:10.1080/09593331808616527

18. A. Ballent, A. Purser, P. de Jesus Mendes, S. Pando, L. Thomsen, Physical transport properties of marine microplastic pollution. *Biogeosciences Discuss.* **9**, 18755–18798 (2012). doi:10.5194/bgd-9-18755-2012

19. C. K. Pham, E. Ramirez-Llodra, C. H. S. Alt, T. Amaro, M. Bergmann, M. Canals, J. B. Company, J. Davies, G. Duineveld, F. Galgani, K. L. Howell, V. A. I. Huvenne, E. Isidro, D. O. B. Jones, G. Lastras, T. Morato, J. N. Gomes-Pereira, A. Purser, H. Stewart, I. Tojeira, X. Tubau, D. Van Rooij, P. A. Tyler, Marine litter distribution and density in European seas, from the shelves to deep basins. *PLOS ONE* **9**, e95839 (2014). doi:10.1371/journal.pone.0095839 Medline

20. L. C. Woodall, A. Sanchez-Vidal, M. Canals, G. L. Paterson, R. Coppock, V. Sleight, A. Calafat, A. D. Rogers, B. E. Narayanaswamy, R. C. Thompson, The deep sea is a major sink for microplastic debris. *R. Soc. Open Sci.* **1**, 140317 (2014). doi:10.1098/rsos.140317 Medline

21. V. Fischer, N. O. Elsner, N. Brenke, E. Schwabe, A. Brandt, Plastic pollution of the Kuril–Kamchatka Trench area (NW pacific). *Deep Sea Res. Part II Top. Stud. Oceanogr.* **111**, 399–405 (2015). doi:10.1016/j.dsr2.2014.08.012

22. W. Courtene-Jones, B. Quinn, S. F. Gary, A. O. M. Mogg, B. E. Narayanaswamy, Microplastic pollution identified in deep-sea water and ingested by benthic invertebrates in the Rockall Trough, North Atlantic Ocean. *Environ. Pollut.* **231**, 271–280 (2017). doi:10.1016/j.envpol.2017.08.026 Medline

23. A. J. Underwood, M. G. Chapman, M. A. Browne, Some problems and practicalities in design and interpretation of samples of microplastic waste. *Anal. Methods* **9**, 1332–1345 (2017). doi:10.1039/C6AY02641A

24. A. R. Thurber, A. K. Sweetman, B. E. Narayanaswamy, D. O. B. Jones, J. Ingels, R. L. Hansman, Ecosystem function and services provided by the deep sea. *Biogeosciences* **11**, 3941–3963 (2014). doi:10.5194/bg-11-3941-2014

25. D. K. Barnes, F. Galgani, R. C. Thompson, M. Barlaz, Accumulation and fragmentation of plastic debris in global environments. *Philos. Trans. R. Soc. London Ser. B* **364**, 1985–1998 (2009). doi:10.1098/rstb.2008.0205 Medline

26. A. Ballent, S. Pando, A. Purser, M. F. Juliano, L. Thomsen, Modelled transport of benthic marine microplastic pollution in the Nazaré Canyon. *Biogeosciences* **10**, 7957–7970 (2013). doi:10.5194/bg-10-7957-2013

27. X. Peng, M. Chen, S. Chen, S. Dasgupta, H. Xu, K. Ta, M. Du, J. Li, Z. Guo, S. Bai, Microplastics contaminate the deepest part of the world's ocean. *Geochem. Perspect. Lett.* **9**, 1–5 (2018). doi:10.7185/geochemlet.1829

28. I. E. Chubarenko, I. E. Esiukova, A. Bagaev, I. Isachenko, N. Demchenko, M. Zobkov, I. Efimova, M. Bagaeva, L. Khatmullina, "Behavior of microplastics in coastal zones" in *Microplastic Contamination in Aquatic Environments* (Elsevier, 2018), pp. 175–223.

29. M. Rebesco, F. J. Hernández-Molina, D. Van Rooij, A. Wåhlin, Contourites and associated sediments controlled by deep-water circulation processes: State-of-the-art and future considerations. *Mar. Geol.* **352**, 111–154 (2014). doi:10.1016/j.margeo.2014.03.011

30. S. Vignudelli, P. Cipollini, M. Astraldi, G. P. Gasparini, G. Manzella, Integrated use of altimeter and in situ data for understanding the water exchanges between the Tyrrhenian and Ligurian Seas. *J. Geophys. Res. Oceans* **105**, 19649–19663 (2000). doi:10.1029/2000JC900083

31. E. Miramontes, P. Garreau, M. Caillaud, G. Jouet, R. Pellen, F. J. Hernández-Molina, M. A. Clare, A. Cattaneo, Contourite distribution and bottom currents in the NW Mediterranean Sea: Coupling seafloor geomorphology and hydrodynamic modeling. *Geomorphology* **333**, 43–60 (2019). doi:10.1016/j.geomorph.2019.02.030

32. G. Dalla Valle, F. Gamberi, Slope channel formation, evolution and backfilling in a wide shelf, passive continental margin (Northeastern Sardinia slope, Central Tyrrhenian Sea). *Mar. Geol.* **286**, 95–105 (2011). doi:10.1016/j.margeo.2011.06.005

33. I. N. McCave, Formation of sediment waves by turbidity currents and geostrophic flows: A discussion. *Mar. Geol.* **390**, 89–93 (2017). doi:10.1016/j.margeo.2017.05.003

34. S. Liubartseva, G. Coppini, R. Lecci, E. Clementi, Tracking plastics in the Mediterranean: 2D Lagrangian model. *Mar. Pollut. Bull.* **129**, 151–162 (2018). doi:10.1016/j.marpolbul.2018.02.019 Medline

35. C. Cencini, Physical processes and human activities in the evolution of the Po delta, Italy. *J. Coast. Res.* **14**, 774–793 (1998).

36. D. A. Kroodsma, J. Mayorga, T. Hochberg, N. A. Miller, K. Boerder, F. Ferretti, A. Wilson, B. Bergman, T. D. White, B. A. Block, P. Woods, B. Sullivan, C. Costello, B. Worm, Tracking the global footprint of fisheries. *Science* **359**, 904–908 (2018). doi:10.1126/science.aao5646 Medline

37. M. Bergmann, V. Wirzberger, T. Krumpen, C. Lorenz, S. Primpke, M. B. Tekman, G. Gerdts, High quantities of microplastic in arctic deep-sea sediments from the HAUSGARTEN observatory. *Environ. Sci. Technol.* **51**, 11000–11010 (2017). doi:10.1021/acs.est.7b03331 Medline

38. A. Sanchez-Vidal, R. C. Thompson, M. Canals, W. P. de Haan, The imprint of microfibres in southern European deep seas. *PLOS ONE* **13**, e0207033 (2018). doi:10.1371/journal.pone.0207033 Medline

39. I. A. Kane, M. A. Clare, Dispersion, accumulation, and the ultimate fate of microplastics in deep-marine environments: A review and future directions. *Front. Earth Sci.* **7**, 80 (2019). doi:10.3389/feart.2019.00080

40. D. J. Piper, P. Cochonat, M. L. Morrison, The sequence of events around the epicentre of the 1929 Grand Banks earthquake: Initiation of debris flows and turbidity current inferred from sidescan sonar. *Sedimentology* **46**, 79–97 (1999). doi:10.1046/j.1365-3091.1999.00204.x

41. M. Azpiroz-Zabala, M. J. B. Cartigny, P. J. Talling, D. R. Parsons, E. J. Sumner, M. A. Clare, S. M. Simmons, C. Cooper, E. L. Pope, Newly recognized turbidity current structure can explain prolonged flushing of submarine canyons. *Sci. Adv.* **3**, e1700200 (2017). doi:10.1126/sciadv.1700200 Medline

42. J. J. Mountjoy, J. D. Howarth, A. R. Orpin, P. M. Barnes, D. A. Bowden, A. A. Rowden, A. C. G. Schimel, C. Holden, H. J. Horgan, S. D. Nodder, J. R. Patton, G. Lamarche, M. Gerstenberger, A. Micallef, A. Pallentin, T. Kane, Earthquakes drive large-scale submarine canyon development and sediment supply to deep-ocean basins. *Sci. Adv.* **4**, eaar3748 (2018). doi:10.1126/sciadv.aar3748 Medline

43. F. Pohl, J. T. Eggenhuisen, I. A. Kane, M. A. Clare, Transport and burial of microplastics in deep-marine sediments by turbidity currents. *Environ. Sci. Technol.* **54**, 4180–4189 (2020). doi:10.1021/acs.est.9b07527 Medline

44. V. Galy, C. France-Lanord, O. Beyssac, P. Faure, H. Kudrass, F. Palhol, Efficient organic carbon burial in the Bengal fan sustained by the Himalayan erosional system. *Nature* **450**, 407–410 (2007). doi:10.1038/nature06273 Medline

45. M. Canals, P. Puig, X. D. de Madron, S. Heussner, A. Palanques, J. Fabres, Flushing submarine canyons. *Nature* **444**, 354–357 (2006). doi:10.1038/nature05271 Medline

46. R. Hurley, J. Woodward, J. J. Rothwell, Microplastic contamination of river beds significantly reduced by catchment-wide flooding. *Nat. Geosci.* **11**, 251–257 (2018). doi:10.1038/s41561-018-0080-1

47. S. J. Hall, The continental shelf benthic ecosystem: Current status, agents for change and future prospects. *Environ. Conserv.* **29**, 350–374 (2002). doi:10.1017/S0376892902000243

48. C. Treignier, S. Derenne, A. Saliot, Terrestrial and marine n-alcohol inputs and degradation processes relating to a sudden turbidity current in the Zaire canyon. *Org. Geochem.* **37**, 1170–1184 (2006). doi:10.1016/j.orggeochem.2006.03.010

49. A. J. Davies, G. C. A. Duineveld, M. S. S. Lavaleye, M. J. N. Bergman, H. van Haren, J. M. Roberts, Downwelling and deep-water bottom currents as food supply mechanisms to the cold-water coral *Lophelia pertusa* (Scleractinia) at the Mingulay Reef Complex. *Limnol. Oceanogr.* **54**, 620–629 (2009). doi:10.4319/lo.2009.54.2.0620

50. D. Xanthos, T. R. Walker, International policies to reduce plastic marine pollution from single-use plastics (plastic bags and microbeads): A review. *Mar. Pollut. Bull.* **118**, 17–26 (2017). doi:10.1016/j.marpolbul.2017.02.048 Medline

51. A. Shields, "Anwendung der Aehnlichkeitsmechanik und der Turbulenzforschung auf die Geschiebebewegung," thesis, Technische Universität Berlin (Preussischen Versuchsanstalt für Wasserbau, 1936).

52. L. C. van Rijn, Sediment transport, part II: Suspended load transport. *J. Hydraul. Eng.* **110**, 1613–1641 (1984). doi:10.1061/(ASCE)0733-9429(1984)110:11(1613)

53. Y. Niño, F. Lopez, M. Garcia, Threshold for particle entrainment into suspension. *Sedimentology* **50**, 247–263 (2003). doi:10.1046/j.1365-3091.2003.00551.x

54. I. Kane, M. A. Clare, E. Miramontes, R. Wogelius, J. J. Rothwell, P. Garreau, F. Pohl, Seafloor microplastic hotspots controlled by deep-sea circulation, Dryad (2020); https://doi.org/10.5061/dryad.tht76hdwf.

55. M. Claessens, S. De Meester, L. Van Landuyt, K. De Clerck, C. R. Janssen, Occurrence and distribution of microplastics in marine sediments along the Belgian coast. *Mar. Pollut. Bull.* **62**, 2199–2204 (2011). doi:10.1016/j.marpolbul.2011.06.030 Medline

56. L. Van Cauwenberghe, A. Vanreusel, J. Mees, C. R. Janssen, Microplastic pollution in deep-sea sediments. *Environ. Pollut.* **182**, 495–499 (2013). doi:10.1016/j.envpol.2013.08.013 Medline

57. J. H. Dekiff, D. Remy, J. Klasmeier, E. Fries, Occurrence and spatial distribution of microplastics in sediments from Norderney. *Environ. Pollut.* **186**, 248–256 (2014). doi:10.1016/j.envpol.2013.11.019 Medline

58. V. Hidalgo-Ruz, L. Gutow, R. C. Thompson, M. Thiel, Microplastics in the marine environment: A review of the methods used for identification and quantification. *Environ. Sci. Technol.* **46**, 3060–3075 (2012). doi:10.1021/es2031505 Medline

59. R. L. Coppock, M. Cole, P. K. Lindeque, A. M. Queirós, T. S. Galloway, A small-scale, portable method for extracting microplastics from marine sediments. *Environ. Pollut.* **230**, 829–837 (2017). doi:10.1016/j.envpol.2017.07.017 Medline

60. B. De Witte, L. Devriese, K. Bekaert, S. Hoffman, G. Vandermeersch, K. Cooreman, J. Robbens, Quality assessment of the blue mussel (*Mytilus edulis*): Comparison between commercial and wild types. *Mar. Pollut. Bull.* **85**, 146–155 (2014). doi:10.1016/j.marpolbul.2014.06.006 Medline

61. P. L. Corcoran, M. C. Biesinger, M. Grifi, Plastics and beaches: A degrading relationship. *Mar. Pollut. Bull.* **58**, 80–84 (2009). doi:10.1016/j.marpolbul.2008.08.022 Medline

62. M. R. Jung, F. D. Horgen, S. V. Orski, V. Rodriguez C., K. L. Beers, G. H. Balazs, T. T. Jones, T. M. Work, K. C. Brignac, S.-J. Royer, K. D. Hyrenbach, B. A. Jensen, J. M. Lynch, Validation of ATR FT-IR to identify polymers of plastic marine debris, including those ingested by marine organisms. *Mar. Pollut. Bull.* **127**, 704–716 (2018). doi:10.1016/j.marpolbul.2017.12.061 Medline

63. N. P. Edwards, H. E. Barden, B. E. van Dongen, P. L. Manning, P. L. Larson, U. Bergmann, W. I. Sellers, R. A. Wogelius, Infrared mapping resolves soft tissue preservation in 50

million year-old reptile skin. *Proc. Biol. Sci.* **278**, 3209–3218 (2011). doi:10.1098/rspb.2011.0135 Medline

64. I. N. McCave, B. Manighetti, S. G. Robinson, Sortable silt and fine sediment size/composition slicing: Parameters for palaeocurrent speed and palaeoceanograpy. *Paleoceanography* **10**, 593–610 (1995). doi:10.1029/94PA03039

65. B. Graca, K. Szewc, D. Zakrzewska, A. Dołęga, M. Szczerbowska-Boruchowska, Sources and fate of microplastics in marine and beach sediments of the Southern Baltic Sea—a preliminary study. *Environ. Sci. Pollut. Res. Int.* **24**, 7650–7661 (2017). doi:10.1007/s11356-017-8419-5 Medline

66. H. A. Leslie, S. H. Brandsma, M. J. M. van Velzen, A. D. Vethaak, Microplastics en route: Field measurements in the Dutch river delta and Amsterdam canals, wastewater treatment plants, North Sea sediments and biota. *Environ. Int.* **101**, 133–142 (2017). doi:10.1016/j.envint.2017.01.018 Medline

67. J. Martin, A. Lusher, R. C. Thompson, A. Morley, The deposition and accumulation of microplastics in marine sediments and bottom water from the Irish continental shelf. *Sci. Rep.* **7**, 10772 (2017). doi:10.1038/s41598-017-11079-2 Medline

68. L. D. K. Kanhai, C. Johansson, J. P. G. L. Frias, K. Gardfeldt, R. C. Thompson, I. O'Connor, Deep sea sediments of the Arctic Central Basin: A potential sink for microplastics. *Deep Sea Res. Part I Oceanogr. Res. Pap.* **145**, 137–142 (2019). doi:10.1016/j.dsr.2019.03.003

69. P. Lazure, F. Dumas, An external–internal mode coupling for a 3D hydrodynamical model for applications at regional scale (MARS). *Adv. Water Resour.* **31**, 233–250 (2008). doi:10.1016/j.advwatres.2007.06.010

70. T. Duhaut, M. Honnorat, L. Debreu, Développements numériques pour le modele MARS. *Contrat Prévimer–Ref* **9**, 211 (2008).

71. F. Léger, C. Lebeaupin Brossier, H. Giordani, T. Arsouze, J. Beuvier, M.-N. Bouin, É. Bresson, V. Ducrocq, N. Fourrié, M. Nuret, Dense water formation in the north-western Mediterranean area during HyMeX-SOP2 in 1/36° ocean simulations: Sensitivity to initial conditions. *J. Geophys. Res. Oceans* **121**, 5549–5569 (2016). doi:10.1002/2015JC011542

72. H. Schlichting, K. Gersten, *Boundary-Layer Theory* (Springer, 2016).